$LMU \ 06/96$

Four fermion final states in e^+e^- annihilation

A. Leike a * †

^aLudwig-Maximilians-Universität, Theresienstr. 37, D-80333 München, Germany

The present status of calculations of four fermion final states is reviewed. Higher order problems arising there are pointed out. Special attention is paid to results obtained in the semi-analytical approach and their limitations and perspectives.

1. Introduction

Four fermion final states are already observed at LEP1 [1]. They are the main final states to be investigated at LEP2 [2]. The two LEP runs planned this year

June/July at
$$\sqrt{s} = 161 \, GeV$$

September/October at $\sqrt{s} = 174 \, GeV$

will give the first opportunity to compare theoretical predictions with the experimental data at the highest energies ever reached in e^+e^- collisions.

The production of two fermions in the final state is quite simple at the Born level. It proceeds through annihilation of gauge bosons in the s channel, figure 1a. For Bhabha scattering, the gauge boson exchange is also possible in the t channel, figure 1b.

Four fermion final states can be created only in higher order processes. They are described by sets of Feynman diagrams, which have a much richer topology. Two diagrams, figure 1c and 1d are essentially new containing the non-abelian interaction of gauge bosons. The diagrams 1e and 1f can be interpreted as the radiation of a fermion pair from the initial and final state of the diagram 1a. Similarly figures 1g and 1h show pair radiation from the diagram 1b. The corresponding diagrams with Higgs exchange are not shown in figure 1. They can be obtained by replacements of a gauge boson with the Higgs at the appropriate places.

The cross sections of four fermion final states

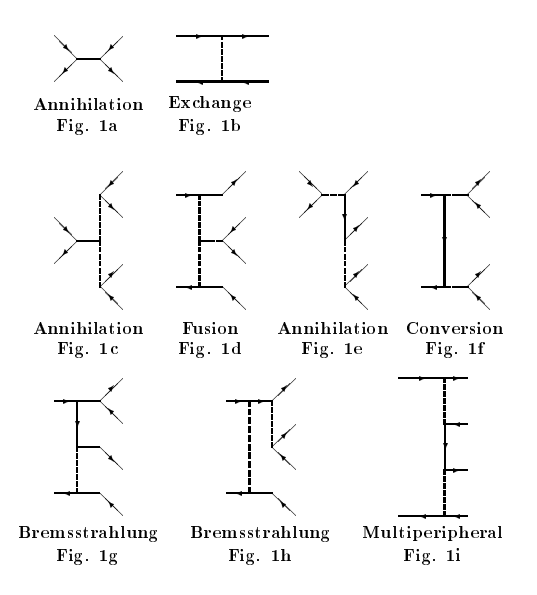


Fig. 1: Topologies of the lowest order Feynman diagrams for $e^+e^- \to f\bar{f}$ and $e^+e^- \to f_1f_2f_3f_4$. The dashed lines represent any allowed gauge boson.

can be of the order of those of fermion pair production due to large factors, which can arise and compensate the additional α^2 .

The diagrams in figures 1c and 1f contain two resonating gauge bosons, which tend to be on mass-shell. They are called signal diagrams for W and Z pair production. Any resonating gauge boson V enhances the cross section by roughly a factor

$$M_V/\Gamma_V \approx 37 \text{ for } V = W \text{ or } Z.$$
 (1)

If the resonating boson is a photon going to $f\bar{f}$, the enhancement factor (without cuts) is

^{*}Partially supported by EC contract CHRX-CT94-0579 †Invited minireview held at "QED and QCD at higher orders", Rheinsberg, April 1996.

 $\ln[s/(m(f) + m(\bar{f}))^2]$. If the photon couples to light fermions, we recover the infrared divergence due to soft photons. We assume that both fermions f, \bar{f} are seen in the detector. This implies that the virtual photon cannot be arbitrarly soft. The diagrams shown in figures 1d, 1e, 1g and 1h are enhanced by only one resonating gauge boson

Diagram 1e is unique because it is the only one, which allows gluon exchange at the tree level. This gives an enhancement by a factor

$$\alpha_s^2(q^2)/\alpha^2 \approx 14^2 \text{ to } 25^2$$
 (2)

depending on the scale q^2 of α_s .

All diagrams with gauge boson exchange in the t channel (figures 1b, 1d, 1g, 1h and 1i) contain collinear singularities. Although they are regularized by the non-zero electron mass, an enhancement factor

$$ln s/m_e^2 \approx 28$$
(3)

remains for every collinear photon in the total cross section. This large factor can be reduced by a cut on the angle between the outgoing $e^+(e^-)$ and the beam axis,

Let us be more explicit and estimate the total cross sections for $e^+e^- \to W^+W^-$ and $e^+e^- \to e^+e^-f\bar{f}$ compared to $e^+e^- \to f\bar{f}$ by collecting only large enhancement factors.

W pair production has a double resonant enhancement. A further enhancement comes from the counting of the possible final states. Fermion pair production results in 5 different quark flavours with three different colors each or in 3 different lepton or neutrino pairs. This adds up to 21 different final states. A W can decay in 2 different quark pairs of 3 different colors each or in 3 different lepton pairs. This gives 9 different final states. We have yet to take into account the combinatorical factor $\sqrt{2}$, which enhances the $W^{\pm} f_1 f_2$ couplings relative to the $Zf\bar{f}$ couplings. This is also the reason, why $\Gamma_Z/\Gamma_W \approx 21/(2\cdot 9)$ and not 21/9. Combined, we get the following additional factor for W pair production compared to fermion pair production:

$$\sigma(e^+e^- \to (WW) \to f_1f_2f_3f_4)$$

$$\approx \sum_{f} \sigma(e^{+}e^{-} \to f\bar{f}) \cdot \alpha^{2} \cdot \frac{(2 \cdot 9)^{2}}{21} \frac{M_{W}^{2}}{\Gamma_{W}^{2}}$$

$$\approx \sum_{f} \sigma(e^{+}e^{-} \to f\bar{f}) \cdot 1.4 \tag{4}$$

After dividing out the threshold factor $\beta = \sqrt{1-4M_W^2/s}$ for W pair production, this crude estimate is correct within a factor 1.5 for $2M_W < \sqrt{s} < 500\,GeV$. For very high energies, the cross section for W pair production becomes larger than the estimate (4) due to terms proportional to $\ln(s/M_W^2)$. The production of two intermediate Z bosons is suppressed by the effective symmetrization arising compared to W pair production.

The cross section of the reaction $e^+e^- \rightarrow e^+e^-f\bar{f}$ is dominated by diagrams shown in figure 1i. All three propagators in the t channel can become singular simultaneously leading to huge enhancement factors. These factors can be estimated starting from the description of the process as a scattering of photons with Weizsäcker-Williams spectrum [3]. Keeping only the leading terms, one gets

$$\sigma(e^{+}e^{-} \to e^{+}e^{-}f\bar{f}) \qquad (5)
\approx \sigma^{QED}(e^{+}e^{-} \to f\bar{f})
\cdot \frac{3\alpha^{2}Q_{f}^{2}}{4\pi^{2}} \frac{s}{m_{f}^{2}} \ln\left(\frac{s}{m_{e}^{2}} \frac{s}{4m_{f}^{2}}\right) \ln\frac{s}{4m_{f}^{2}} \ln\frac{4m_{f}^{2}}{m_{e}^{2}}.$$

For f = b, we get at $\sqrt{s} = 200 \, GeV$

$$\sigma(e^{+}e^{-} \to e^{+}e^{-}b\bar{b})$$

$$\approx \sigma^{QED}(e^{+}e^{-} \to b\bar{b}) \cdot 3 \approx 2.5 \, pb. \tag{6}$$

This is less than a factor 2 off from the exact result, see figure 13 in [3].

All four fermion final states can be classified according to the topologies of Feynman diagrams entering the process. The number of the Feynman diagrams involved in different processes with charged current exchange is shown in table 1, while table 2 contains final states, which are produced by the exchange of neutral gauge bosons only. Potential diagrams with Higgs exchange are not counted. Diagrams coming from different contributions of quark mixing are counted. Final states indicated in **bold** contain only the topologies of figures 1e and 1f. In the case of charged

currents, the topology 1c has to be added. These charged current processes are usually referred as CC9, CC10 or CC11 processes. Numbers in italics indicate final states, which belong to table 1 and table 2. The CC43 and CC19 (identical to NC43 and NC19) processes are described only by the topologies of the **bold** processes. However, here new structures in the interferences appear. The CC56 (NC56) process involve all topologies. All remaining processes contain electrons or electron neutrinos in the final state allowing gauge boson exchange in the t channel. The corresponding numbers are written in roman. They contain all topologies simultaneously, except diagram 1d, which demands at least one electron neutrino in the final state. Final states with identical final fermions are given in typewriter. They require additional contributions to insure Pauli antisymmetrization.

	$\bar{d}u$	$\bar{s}c$	$\bar{e}\nu_e$	$\bar{\mu} u_{\mu}$	$\bar{ au} u_{ au}$
$d\bar{u}$	43	11	20	10	10
$e\bar{\nu}_e$	20	20	56	18	18
$\mu \bar{\nu}_{\mu}$	10	10	18	19	9

Tab. 1: Number of Feynman diagrams for CC type final states, see [25].

	$ar{d}d$	$\bar{u}u$	$\bar{e}e$	$\bar{\mu}\mu$	$\bar{\nu}_e \nu_e$	$ar{ u}_{\mu} u_{\mu}$
$\bar{d}d$	4.16	43	48	24	21	10
$\bar{s}s, \bar{b}b$	32	43	48	24	21	10
$\bar{u}u$	43	4.16	48	24	21	10
$\bar{e}e$	48	48	4.36	48	56	20
$\bar{\mu}\mu$	24	24	48	4.12	19	19
$ar{ au} au$	24	24	48	24	19	10
$\bar{\nu}_e \nu_e$	21	21	56	19	4.9	12
$\bar{ u}_{\mu} u_{\mu}$	10	10	20	19	12	4.3
$\bar{\nu}_{ au} u_{ au}$	10	10	20	10	12	6

Tab. 2: Number of Feynman diagrams for NC type final states, see [24].

2. Higher order corrections

Four fermion final states can be produced with cross sections of several pb. With an integrated luminosity of $500pb^{-1}$ per year, the expected experimental precision for some cross sections is

about 1%. It has to be met by theoretical predictions, which have errors of 0.5% or less. Hence, higher order corrections have to be included.

2.1. QED corrections

The complete QED corrections to four fermion final states are not known. One could simplify the problem for W pair production considering corrections to the signal diagrams figures 1c and 1f only. As an important step, this was done in the case of on-shell W's [4]. For off-shell W's, the complete correction is not known.

In the following, the Coulomb singularity and initial state corrections are mentioned.

Coulomb singularity

The Coulomb singularity [5] arises from long range electromagnetic interactions between the produced massive charged particles. For W pair production, we get the correction

$$\sigma^{Coul} = \sigma^0 \left(1 + \frac{\alpha \pi}{2\beta} \right) \tag{7}$$

to the Born cross section σ^0 , which diverges near threshold where the velocity of the W's $\beta = \sqrt{1-4M_W^2/s}$ approaches zero. It indicates that perturbation theory is not applicable in this region. Fortunately, the non-zero width Γ_W and a slight off-shell production of the W's regularize the singularities in equation (7). The numerical effect can exceed 6% of the total cross section near threshold [6, 7]. Therefore, the Coulomb correction has to be inleuded.

Formula (7) also applies for QED and QCD corrections to pair production of massive fermions as it appears in the diagrams 1d-1h. This is well known from final state corrections to the diagram 1a at LEP1 [8]. The problems can be cured by a calculation in the limit of massless fermions or by a cut on the invariant mass of the heavy fermion pairs. Such a cut is desirable for quark pairs in any case to avoid non-perturbative bound state regions.

Initial state corrections

Initial state QED corrections to off-shell W pair production are calculated in [9]. They reach several % near the WW threshold. In such calculations a problem arises because it is not clear

how to separate weak corrections from QED corrections and initial state QED corrections in a unique and gauge invariant way. This separation problem is solved by the current splitting technique [9], in which the chargeless neutrino exchanged in the t channel is divided into two charge flows of opposite sign. Now the charge flows of the initial and final states are separated. and gauge invariance is ensured as it is in the case of Z pair production. The resulting initial state QED corrections can be split into universal contributions, which are described by the same flux function as known from annihilation diagrams in the case of LEP 1 physics, and into non-universal contributions depending on the particular process. The non-universal contributions to off-shell W and Z production are numerically small for LEP 2 energies. They are suppressed by a factor s_1s_2/s^2 , where $s_{1,2}$ are the invariant energy flows through the W's (Z's) [9, 10]. The smallness of the non-universal corrections cannot be taken for granted, but has to be proven for any particular process.

The universal corrections lead to handy formulae for initial state corrections to cross sections of W and Z pair production,

$$\sigma^{ISR}(s) = \int_{s'^{-}}^{s} \frac{\mathrm{d}s'}{s} \sigma^{0}(s') \rho(s'/s). \tag{8}$$

Alternatively, initial state radiation can be taken into account by the structure function approach [11]. It assumes that both colliding photons have energies degraded by radiated collinear photons,

$$\sigma^{ISR}(s) \qquad (9)$$

$$= \int_{x_1^-}^1 dx_1 \int_{x_2^-}^1 dx_2 D(x_1, s) D(x_2, s) \sigma^0(x_1 x_2 s).$$

The flux function (FF) $\rho(s'/s)$ and the structure function (SF) D(x,s) contain information about real and virtual corrections. Further details can be found, for example, in [7] or [12].

2.2. Electroweak corrections

Complete one-loop corrections to four fermion processes would be the best task to get more accurate descriptions of these cross sections. Unfortunately, this calculation is very complex [13] and done only for on-shell W's [4].

In this paragraph, only electroweak corrections connected with the finite widths of gauge bosons are mentioned.

At lowest order, a particle V has no width, i.e. its propagator D_V is proportional to $D_V \sim [q^2 - M_V^2]^{-1}$, where q^2 is the momentum transfer through the particle of mass M_V .

Massive gauge bosons are unstable having a non-negligible decay width. The required precision at the energy range of LEP 2 demands the inclusion of a finite width. Although the inclusion of a width for particles in the t channel is not physical, the simplest possibility is the inclusion of the constant on-shell decay width Γ_V everywhere in the propagator, $D_V \sim [q^2 - M_V^2 + iM_V\Gamma_V]^{-1}$.

The next step of accuracy, which cures this deficiency, is to take into account the natural energy dependence of the width arising from self-energy insertions into the boson propagator. Present and future experiments are sensitive to the difference of these handlings of the width [14, 15], even at the limit of very high energies.

A finite width in the propagator implies the partial inclusion of contributions, which are of higher order in perturbation theory. Unfortunately, the symmetries of a theory (as gauge invariance) are only respected in a fixed order of perturbation theory. Hence, the inclusion of a non-zero width leads to gauge dependent cross sections. Although the gauge dependent terms are of higher order in perturbation theory, they can be enhanced by large kinematical factors as s/m_e^2 in the reaction $e^+e^- \to e^-\bar{\nu}_e u\bar{d}$, see [16]. Therefore, finite widths must be included with care. Different approaches for the restoration of gauge invariance have been proposed, among them the Laurent expansion of the matrix element and the inclusion of projection operators 17] or the inclusion of certain higher order contributions [18].

2.3. QCD corrections

QCD corrections give sizeable contributions to distributions and cross sections. They are known from LEP 1 for the production of *pairs* of (heavy) quarks [8]. They are under investigation for *four quarks* in the final state [19].

QCD corrections enter the width of the Z,W and the Higgs. For the case of Γ_W , QCD corrections can reach several %, see [20]. Most of the QCD corrections to the Higgs width can be absorbed into the running quark masses evaluated at the scale of the Higgs mass. They lead to values for $m_b(M_H)=2.9\,GeV$ and $m_c(M_H)=0.6\,GeV$ [21], which deviate substantially from the corresponding pole masses.

2.4. Theoretical uncertainties

The theoretical uncertainties are extensively discussed in the different contributions to [2]. Here, we only give some of them in a telegraphic style.

QED corrections:

- The initial state QED corrections to all Born cross sections presented in [2] are calculated by the FF or by the SF approach. The validity of these approximations is proven only for W and Z pair production and for annihilation diagrams. For other processes it is not known, whether the non-universal corrections are small enough to be neglected. Even for W and Z pair production, they reach 0.3% at LEP 2 energies and rise above 1% at $1\,\text{TeV}$ [9,10].
- The FF is derived after an average over all phase space variables except the two invariant energy flows $s_{1,2}$ through the W's or Z's. For distributions or cuts in parameters different from s_1 and s_2 (i.e. angular cuts, cuts on energies of single particles), it depends in general on the additional parameters. This is known from LEP 1, where the angular-dependent FF for annihilation diagrams is derived [22]. The dependence on the distribution parameter disappears only for soft photon radiation. Therefore, the theoretical errors of observables, which favor hard photon radiation can become very large. Fortunately, these observables have small cross sections because QED favors soft photon radiation.
- We now assume that the FF and SF approaches work perfectly to all orders of perturbation theory. We can then use our knowledge about these functions beyond the leading order and study the changes of cross sections. This relative change reaches 0.5% [20] giving an idea about the effect

of higher order QED corrections.

QCD corrections:

- A calculation of complete QCD corrections to four fermion processes is not done. The resulting uncertainty can be estimated in the following simple example: W pair production with four quarks in the final state involves diagram 1e with gluon exchange at the Born level. The diagram favors soft gluons. The minimal momentum transfer through the gluon is usually defined by cuts. The scale q of $\alpha_s(q^2)$ in these contributions is not known exactly. An uncertainty of 20% in the scale q leads to an uncertainty of 10% in $\alpha_s^2(q^2)$ for $q \approx 10 \, GeV$. If the diagram 1e would contribute 10% to the total cross section, this scale uncertainty would transform to an error of 1% in the total cross section. If the cuts allow smaller q^2 , $\alpha_s(q^2)$ and its uncertainty become larger. This simple example illustrates the dependence of QCD corrections on kinematical cuts.
- The running quark masses in Higgs decay depend on $\alpha_s(M_Z)$. The resulting uncertainties are shown in table 3 in [21]. They reach several %. They transform into uncertainties of predictions for production cross sections of Higgs Bosons being proportional to the square of these masses.
- The interface between partonic cross sections and hadronization procedures and the hadronization procedures itself introduce theoretical uncertainties.

Weak corrections

Gauge invariance can be restored in calculations with finite widths by different methods. The arising numerical difference is studied for the process $e^-e^+ \rightarrow e^-\bar{\nu}_e u\bar{d}$ in the second reference of [18] and found to be about 0.5%. The disagreement between the different methods is expected to be larger near threshold [13].

Final remark

The estimation of theoretical errors is a highly subjective task. These errors can be reduced only by future higher order calculations. Remembering that not all theoretical errors are equally important in all observables, we conclude that the present theoretical accuracy probably meets the

precision expected in the first year at LEP 2. It has certainly to be improved in the future.

3. Codes and algorithms

3.1. Existing codes

Event generators for four fermion final states are described in detail in volume 2 of reference [2]. They use different algorithms for the evaluation of the squared matrix elements, phase space integration and mapping of singularities. Numerical comparisons between the programs gave a nice agreement.

It follows a list of the available codes and its authors.

Monte Carlo Programs:

- ALPHA (F. Caravaglios, M. Moretti)
- CompHep 3.0 (E. Boos, et al.)
- ERATO (C.G. Papadopoulos)
- EXCALIBUR (F.A. Berends, R. Kleiss, R. Pittau)
- grc4f 1.0 (J. Fujimoto, et al.)
- KORALW 1.03 (M. Skrzypek, S. Jadach, W. Płaczek, Z. Was)
- LEPWW (F.C. Erné)
- LPWW02 (R. Miquel, M. Schmitt)
- PYTHIA 5.719 / JETSET 7.4 (T. Sjöstrand)
- WOPPER1.4 (H. Anlauf, T. Ohl)
- WPHACT (E. Accomando, A. Ballestrero)
- WWF 2.2 (G.F. van Oldenborgh)
- WWGENPV/HIGGSPV (G. Montagna, O. Nicrosini, F. Piccinini)

Other codes:

- GENTLE/4fan (D. Bardin, D. Lehner, A. Leike, T. Riemann), Semi-analytical code
- WTO (G. Passarino), multi-dimensional deterministic integration

3.2. Comparison between the Monte Carlo the and semi-analytical approach

Many different topologies of Feynman diagrams are involved in calculations of four fermion processes leading to a rather singular matrix element. It has to be integrated over the 8-dimensional phase space. In the case of absence of transversal beam polarization, one degree of freedom, the rotation around the beam axis, is trivial. We

are left with a 7-dimensional phase space integration. In the semi-analytical (SA) approach, most of the phase space integrations are done analytically. The remaining integrals are calculated numerically. In the Monte Carlo (MC) approach, all integrals are taken numerically.

As shown in section 2, kinematical cuts are needed to reject threshold regions of massive fermion pairs because they are not described by perturbation theory. Additional angular and energy cuts are required to ensure the detection of four final particles in a real detector. Finally, a real detector has wholes, which are planned (i.e. for cables and support) and those which arise spontaneously (i.e. damaged and dead sectors). These individual properties have to be inlcuded into a data analysis. There is an additional physical motivation for cuts to separate interesting events from the background.

Having in mind these requirements, it is obvious that one needs a MC event generator. It is most flexible in kinematical cuts and can be connected with detector simulations and hadronization procedures.

On the other hand, fits require fast and accurate programs. The overall accuracy (which consists of theoretical uncertainties and numerical uncertainties) must not be larger than half of the experimental error. Remembering the present theoretical errors, it follows that the numerical uncertainty should be considerably smaller than the experimental error. Demanding that a fit to future data should be finished rather in 1 to 10 days and not in 10 to 100 days, and assuming 100 to 1000 cross section calculations for one fit, one can estimate the calculation speed and accuracy of a code, which is useful for fits: Such a code should calculate one cross section with an numerical accuracy of $\leq 0.1\%$ in less than 15 minutes on computers already available today. The higher speed of future computers will probably be eaten by the implementation of future theoretical results needed to decrease the theoretical errors.

These requirements can be met by a SA code. In the simplest case of the NC32 processes (all **bold** final states in table 2), the typical calculation time is 30s with a numerical accuracy of 0.1% and with QED corrections included by the

FF approach. This time can vary by a factor 3 depending on the cuts and on the final state. The calculation time for CC11 processes (all **bold** final states in table 1) is about 3 times longer due to the longer analytical formulae involved. The codes of GENTLE/4fan distributed during the LEP 2 workshop are much slower. This will be improved with an update at the end of this year.

SA codes are not as flexible as MC's allowing only the calculations of a limited number of distributions. However, they establish a benchmark for MC's because SA codes have an inherently much smaller numerical error. Unfortunately, the SA method can fail for certain processes. For details, see the next section.

The calculation time of SA and MC programs depends on the numerical accuracy ε required. In the SA approach, we have an additional dependence on the dimension d of the numerical integration and on the order r of the numerical integration algorithm:

MC:
$$t \sim \varepsilon^{-2}$$

SA: $t \sim \varepsilon^{-d/r}$ (10)

A few remarks are in order inspecting relations (10):

- \bullet In practice, the calculation time for MC's depends on d because the integrand cannot be mapped to a completely flat function.
- High accuracy demands large calculation times in the MC approach. The difference between $\varepsilon=1\%$ and $\varepsilon=0.1\%$ has to be paid by a factor 100 in computer time.
- In the SA approach, we have r=5 for Simpson's rule. More sophisticated algorithms with larger r don't necessarily lead to shorter calculation times because their errors are proportional to higher derivatives of the integrand.
- SA codes can easily achieve a high accuracy. They are very fast for small d. They fail for large d. In practice, the calculation time increases by more than a factor 10 for every additional integration. We have d=2,3,4 or 5 in GENTLE/4fan for calculations of Born cross sections, QED FF corrected cross sections, QED SF corrected cross sections, QED SF corrected angular distributions. A calculation time below 15 min seems to be possible for d=3 for all solvable processes, and for

d=4 for selected processes only.

4. The semi-analytical approach

SA calculations result to nice analytical formulae, which depend only on the input parameters and on the remaining integration variables. These formulae show symmetries, which allow a deeper physical understanding of the underlying process.

Specific four fermion processes are given by the imaginary part of three-loop diagrams. Therefore, some formulae obtained in the SA approach agree with results of three-loop calculations. However, one has to admit flavour identification in the four fermion final states. Therefore, one is not summing over complete weak multiplets. Furthermore, one is not interested in a complete analytical phase space integration because one wants to calculate distributions and apply cuts.

In contrast to the MC, the SA approach can distinguish analytical zeros from contributions, which are multiplied by (very) small factors. This found an interesting application in the discussion of the interferences in SM Higgs production [23] and can be extended to SUSY Higgs production.

4.1. Cross sections, distributions and cuts

So far, the SA approach [9, 24, 23, 25] uses the following parametrization of the phase space ³:

$$d\Omega = \prod_{i=1}^{4} \frac{d^{3}p_{i}}{2p_{i}^{0}} \delta^{4}(k_{1} + k_{2} - \sum_{i=1}^{4} p_{i})$$

$$= \frac{\sqrt{\lambda(s, s_{1}, s_{2})}}{8s} \frac{\sqrt{\lambda(s_{1}, m_{1}^{2}, m_{2}^{2})}}{8s_{1}}$$

$$\times \frac{\sqrt{\lambda(s_{2}, m_{3}^{2}, m_{4}^{2})}}{8s_{2}} ds_{1} ds_{2} d\Omega_{0} d\Omega_{1} d\Omega_{2},$$
(11)

 k_1 and k_2 are the four-momenta of the initial electron and positron. The fermions f_i in the final state have four-momenta p_i and masses m_i . The invariants s, s_1 , and s_2 are

$$s = (k_1 + k_2)^2,$$

 $s_1 = (p_1 + p_2)^2, \quad s_2 = (p_3 + p_4)^2.$ (12)

³Other parametrizations are considered for different topologies of Fevnman diagrams.

One has to substitute $d\Omega_0 = 2\pi d\cos\theta_0 = 2\pi dc_0$ to integrate over the rotation angle around the beam axis. θ_0 is the angle between the vectors $(\vec{p}_1 + \vec{p}_2)$ and \vec{k}_1 . The spherical angles of the momenta \vec{p}_1 and \vec{p}_2 (\vec{p}_3 and \vec{p}_4) in their rest frames are Ω_1 (Ω_2): $d\Omega_i = d\cos\theta_i d\phi_i = dc_i d\phi_i$. The kinematical ranges of the integration variables are:

$$(m_1 + m_2)^2 \le s_1 \le (\sqrt{s} - m_3 - m_4)^2,$$

 $(m_3 + m_4)^2 \le s_2 \le (\sqrt{s} - \sqrt{s_1})^2,$
 $-1 \le c_i \le 1,$
 $0 \le \phi_i \le 2\pi, \quad i = 0, 1, 2.$ (13)

Usually, the squared matrix element is integrated over all six angles c_i , ϕ_i . The remaining two integrations are done numerically. As a result, the cross section is obtained in the following form:

$$\sigma(s) = \int_{s_{2}^{-}}^{s_{2}^{+}} ds_{2} \int_{s_{1}^{-}}^{s_{1}^{+}} ds_{1} \frac{d^{2}\sigma}{ds_{1}ds_{2}}$$
 (14)

The boundaries of the integrations $s_{1,2}^{\pm}$ allow the implementation of cuts in s_1 and s_2 . These cuts are very important to separate intermediate photons, Z's, W's and Higgs bosons in the diagrams 1c and 1f from the background. The double differential cross section factorizes,

$$\frac{d^2\sigma}{ds_1ds_2} = \sum_i C_i(e, f_1, f_2, f_3, f_4, s, s_1, s_2) \times G_i(s, s_1, s_2), \tag{15}$$

where $C_i(\ldots)$ are functions depending on the couplings and the invariants and $G_i(\ldots)$ are kinematical functions resulting from the six-fold analytical integration. They depend on the invariants only. The summation runs over the interferences of different topologies. The double differential cross sections allow the calculation of the distributions

$$\frac{d\sigma}{ds_1}, \quad \frac{d\sigma}{ds_2}, \quad \frac{d\sigma}{dE_{12}}, \tag{16}$$

where E_{12} is the sum of the energies of the particles f_1 and f_2 ,

$$E_{12} = p_{10} + p_{20} = \frac{s + s_1 - s_2}{2\sqrt{s}}.$$
 (17)

Cuts are possible on all parameters in equation (16) simultaneously.

To be more differential, the integration over c_0 can be left for numerical integration [26]. The results are triple differential cross sections,

$$\frac{d^3\sigma}{ds_1ds_2dc_0} = \sum_i C_i(e, f_1, f_2, f_3, f_4, s, s_1, s_2) \times G_i(s, s_1, s_2, c_0)$$
(18)

with the remaining numerical integrations

$$\sigma(s) = \int_{s_{2}^{-}}^{s_{2}^{+}} ds_{2} \int_{s_{1}^{-}}^{s_{1}^{+}} ds_{1} \int_{c_{0}^{-}}^{c_{0}^{+}} dc_{0} \frac{d^{3}\sigma}{ds_{1}ds_{2}dc_{0}}.$$
(19)

The parameters s_1, s_2 and c_0 allow the construction of additional distributions,

$$\frac{d\sigma}{dc_0}$$
, $\frac{d\sigma}{dp_{12}^T}$, $\frac{d\sigma}{dy_{12}}$, (20)

where p_{12}^T is the sum of the transversal momenta of the particles f_1 and f_2 against the beam axis, and y_{12} is the rapidity related to p_{12}^T . The new parameters depend on s_1, s_2 and c_0 only,

$$p_{12}^{T} = \sqrt{E_{12}^{2} - (m_{1} + m_{2})^{2}} \sqrt{1 - c_{0}^{2}}$$

$$\tanh y_{12} = c_{0} \sqrt{1 - (m_{1} + m_{2})^{2} / E_{12}^{2}}.$$
 (21)

Again, cuts are possible on all parameters in equations (16) and (20) simultaneously.

All distributions listed in equations (16) and (20) can be calculated with initial state radiation too. This is possible because s_1 and s_2 are invariants, and c_0 can be reconstructed after a boost due to photon radiation from the initial state without use of Ω_1 and Ω_2 .

Alternatively, one of the parameters c_1 or c_2 can be left for numerical integration. The corresponding cross section formulae are identical to (18) and (19) with c_0 substituted by c_1 or c_2 . No new functions $C_i(\ldots)$ and $G_i(\ldots)$ appear in the case of NC32 processes. The distributions

$$\frac{d\sigma}{dp_{i0}}, \quad \frac{d\sigma}{dp_i^T}, \quad \frac{d\sigma}{dy_i}, \quad \frac{d\sigma}{dc_{12}}, \quad i = 1, 2$$
 (22)

are now calculable because

$$p_{10} = \frac{(s_1 + m_1^2 - m_2^2)(s + s_1 - s_2)}{4s_1\sqrt{s}}$$

$$+c_{1} \frac{\sqrt{\lambda(s_{1}, m_{1}^{2}, m_{2}^{2})\lambda(s, s_{1}, s_{2})}}{4s_{1}\sqrt{s}},$$

$$p_{1}^{T} = \sqrt{p_{10}^{2} - m_{1}^{2}} \sqrt{1 - c_{1}^{2}} = p_{2}^{T},$$

$$\tanh y_{1} = c_{1} \sqrt{1 - m_{1}^{2}/p_{10}^{2}} \text{ and } (23)$$

$$c_{12} = -\frac{1 - (1 - c_{1}^{2})\lambda(s, s_{1}, s_{2})/(4ss_{1})}{1 + (1 - c_{1}^{2})\lambda(s, s_{1}, s_{2})/(4ss_{1})}.$$

depend on s_1, s_2 and c_1 only. p_1^T is the transversal momentum against the $\vec{p}_1 + \vec{p}_2$ axis, y_1 is the rapidity related to p_1^T , and c_{12} is the cosine of the angle between \vec{p}_1 and \vec{p}_2 . For simplicity, the formula for c_{12} is given only in the massless limit. As in the case with open c_0 , cuts are possible to the parameters in equations (16) and (22) simultaneously. Similar formulae can be written for the case where c_2 is left for numerical integration.

The distributions (23) can be calculated in the SA approach only at the Born level. The reason is that $c_1(c_2)$ cannot be reconstructed after a boost of the subsystem due to photon radiation without knowledge of c_0 and $\phi_1(\phi_2)$. Unfortunately, these angles are already integrated out.

4.2. Limitations and perspectives

Presently, only final states marked in **bold** in tables 1 and 2 (NC32, CC11) are treated in the SA approach. Final states printed in the tables in roman (NC48, CC20) are under investigation [27]. The NC43, NC19 (CC43, CC19) can certainly be treated.

All processes with identical particles in the final state (NC 4·36) given in table 2 in typewriter cannot be treated with cuts on $s_1 = (p_1 + p_2)^2$ and $s_2 = (p_3 + p_4)^2$. These cuts imply the same cuts on $\bar{s}_1 = (p_1 + p_4)^2$ and $\bar{s}_2 = (p_3 + p_2)^2$ because the identical final particles are indistinguishable. They have to be calculated with a phase space parametrization, which has the four invariants $s_1, s_2, \bar{s}_1, \bar{s}_2$ as integration parameters. Unfortunately, the transformation to these parameters is described by general polynomials of fourth power, which have to be inverted.

The four jet cross section with two quarks and two gluons in the final state [28] has to be added incoherently to the NC32 and CC11 processes. All soft singularities can be eliminated by a cut

on the invariants s_1 and s_2 . The collinear singularities are regularized by a finite quark mass m_q . However, the differential cross section is enhanced by a factor s/m_q^2 for every gluon, which is collinear with a quark. Experimentally, one can discover a four jet event only, if the jets are separated by a minimal angle. Such an angular cut is not possible in the SA approach. This shows another limitation of this calculation scheme. The problem arises already in four quark final final states but without collinear enhancement.

Finally, I would like to add some remarks about possible future SA calculations.

The inclusion of anomalous couplings is possible for the CC11 process [29]. The treatment of SUSY Higgs cross section is possible everywhere, where the corresponding topology with SM gauge bosons can be calculated. This includes the schannel Higgs diagrams in muon colliders. Four fermion final states in e^-e^- collisions can be calculated, if the corresponding topologies are calculable in e^+e^- collisions. $\gamma e(\gamma \gamma)$ collisions demand one more integration for every photon in the initial state. This complication could be compensated by the missing QED corrections from the initial photon. The inclusion of SUSY processes with four fermions in the final states is interesting. Unfortunately, many SUSY processes lead to six fermion final states.

To summarize this section, we emphasize that the SA and MC approach are complementary. Both approaches have advantages and disadvantages. Both are needed at different places in a future data analysis.

5. Summary

The physics of four fermion final states is much richer than that of two fermion final states. The calculation of four fermion cross sections with a theoretical error below 0.5% is challenging.

In general, complicated kinematical cuts are required already for Born cross sections to ensure the applicability of perturbation theory and to separate interesting events from the background. Radiative corrections are necessary. The codes used in fits to future data must be fast and accu-

rate.

Not all these features can be met by a code based on *one* calculation scheme only. Flexible Monte Carlo programs and fast semi-analytical programs together could fulfill all requirements.

Present codes probably meet the experimental precision expected at LEP 2 *this* year. Theoretical errors certainly must be reduced to meet the accuracy of the LEP 2 data in the future.

REFERENCES

- ALEPH Collaboration (D. Buskulic et al.), Z.Phys.C66 (1995) 3.
- 2. G. Altarelli, T. Sjöstrand, F. Zwirner (eds.), Proceedings of the Workshop *Physics at LEP 2*, CERN 96–01.
- 3. F. Boudjema, B. Mele (conv.), in Ref. [2], vol. 1, p. 207.
- M. Böhm et al., Nucl. Phys. B304 (1988)
 463; W. Beenakker, K. Kołodziej, T. Sack,
 Phys. Lett. B262 (1991) 125; J. Fleischer,
 K. Kołodziej, F. Jegerlehner, Phys. Rev. D47 (1993) 830.
- A. Sommerfeld, Atombau und Spektrallinien (Vieweg, Braunschweig, 1939) Bd. 2; A.D. Sakharov, JETP 18 (1948) 631.
- V.S. Fadin, V.A. Khoze, A.D. Martin, Phys. Lett. B311 (1993) 311; B320 (1994) 141.
- D. Bardin, W. Beenakker, A. Denner, Phys. Lett. **B317** (1993) 213.
- J. Jersak, E.L. Laermann, P.M. Zerwas, Phys. Rev. **D25** (1981) 1218, E: **D36** (1987) 310;
 Phys. Lett. **B98** (1981) 363; A.B. Arbuzov,
 D.Yu. Bardin, A. Leike, Int. J. Mod. Phys. Lett. **A7** (1992) 2029, E: **A9** (1994) 1515.
- D. Bardin, M. Bilenky, A. Olchevski, T. Riemann, Phys. Lett. **B308** (1993) 403; E: *Phys. Lett.* **B357** (1995) 725; complete revised version: hep-ph/9507277.
- D. Bardin, D. Lehner, T. Riemann, DESY 96–028 (1996), hep-ph/9602409; D. Lehner, Ph.D. thesis, Humboldt-Universität zu Berlin (1995), DESY-Zeuthen 95-07, hep-ph/9512301.
- E.A. Kuraev, V.S. Fadin, Sov. J. Nucl. Phys. 41 (1985) 466.
- 12. F.A. Berends, R. Pittau, R. Kleiss, Nucl.

- Phys. **B426** (1994) 344, hep-ph/9405398.
- A. Aeppli, G.J. van Oldenborgh, D. Wyler Nucl. Phys. **B428** (1994) 126, hep-ph/9312212.
- F.A. Berends, G. Burgers, W. Hollik, W.L. van Neerven, Phys. Lett. **B203** (1988) 177;
 D.Y. Bardin, A. Leike, T. Riemann, M. Sachwitz, Phys. Lett. **B206** (1988) 539.
- W. Beenakker, A. Denner, Int. J. Mod. Phys. A9 (1994) 4837.
- F.A. Berends, G.B. West, Phys. Rev. **D1** (1970) 122.
- 17. R.G. Stuart, UM-TH-96-05, hep-ph/9603351.
- U. Baur, D. Zeppenfeld, Phys. Rev. Lett. **75** (1995) 1002; E.N. Argyres, et al., Phys. Lett. **B358** (1995) 339.
- 19. R. Pittau, private communication.
- D. Bardin, R. Kleiss (conv.) et al., in Ref. [2], v. 2, p.3.
- M. Carena, P. Zerwas (conv.) et al., in Ref.
 [2], v. 1, p.351. M.L. Mangano, G. Ridolfi (conv.) et al., in Ref.
 [2], v. 2, p.299.
- D. Bardin, M. Bilenky, A. Chizhov, A. Sazonov, O. Fedorenko, T. Riemann, M. Sachwitz, Nucl. Phys. B351 (1991) 1.
- D. Bardin, A. Leike, T. Riemann, hepph/9504204, Phys. Lett. B353 (1995) 513.
- D. Bardin, A. Leike, T. Riemann, hepph/9410361, Phys. Lett. B344 (1995) 383.
- D. Bardin, T. Riemann, DESY 95–167 (1995), hep-ph/9509341, Nucl. Phys. B462 (1996) 3.
- A. Leike, in: B. Kniehl (ed.), Proceedings of the Workshop Perspectives for electroweak interactions in e⁺e⁻ collisions, Ringberg, Germany, February 1995 (World Scientific, Singapore, 1995), p. 121, hep-ph/9504358.
- 27. D. Bardin, J. Biebel, A. Leike, T. Riemann, under investigation.
- 28. M. Jack, A. Leike, in progress.
- 29. J. Biebel, T. Riemann, in progress; a preliminary Fortran program exists.